H E R ● N

Contents

**Micro- and macromechanical behaviour of
steel fibre reinforced mortar in tension**
Dr. Ir. P. Stroeven

**A concrete beam reinforced with bars and
steel fibres in pure bending**
Prof. Dr.-Ing. H. W. Reinhardt

**Experiments on concrete beams reinforced
with conventional reinforcement and steel
fibres subjected to fatigue loading**
Ir. H. A. Körmeling

Publications in HERON since 1970

Micro- and macromechanical behaviour of steel fibre reinforced mortar in tension

Dr. Ir. P. Stroeven

1 Introduction

Methods for the accurate estimation of the fibre contribution to the load-bearing and other mechanical properties of structural elements, fabricated from fibre reinforced cementitious matrices (FRC), constitute a necessary basis for intelligent design of such elements. Generally, the experimental investigations that underlie proposed methods encompass pull-out tests on single fibres. By using more fibres, the so-called group effect – a recognized phenomenon in pile foundations – can additionally be studied. To estimate the relative contribution of non-aligned fibres in a group, pairs of fibres, obliquely embedded with respect to the applied loading direction, have been pulled-out from the cementitious matrix [Naaman and Shah, 1975; Maage, 1976]. Since the fibre contribution in the precracked state can suitably be approximated by means of a simple "law of mixtures", the post cracking behaviour deserves primary attention. In dealing with the structure-sensitive phenomenon of crack development, which is associated with the process of structural degradation, the heterogeneity of the materials becomes a leading parameter. It is relevant to distinguish between heterogeneity with respect to location and orientation of the fibres. In both cases one has to be aware in practical situations of the possible joint occurrence of random as well as systematic variations. It is demonstrated that compaction-induced segregation as well as partial orientation of the fibre structure can occur in the specimens [Stroeven, 1979; Stroeven, 1980a]. Moreover, the outer surfaces (of the mould) will locally introduce preferred orientation effects as well [Stroeven, 1978; Stroeven, 1980b]. The stochastic character of the spatial dispersion of the fibres may be assumed to be governed by a Poisson process. Systematic effects, however, must be experimentally investigated in the actual situation to facilitate estimation of this effect on the macromechanical properties.

A representative microstructural element of a specimen in the post-cracking stage should obviously be composed of a part of matrix material containing one or more fibres bridging the crack. The structure of the fibres that cross the crack has less trivial morphological features than generally accepted. Even for a spatially random fibre dispersion it can easily be shown that sampling by a crack (or plane) will yield a subset of fibres with preferred orientation under 45° with the crack plane. This makes integration towards a higher dimensional level a more complicated step than commonly recognized. The as yet unknown details of the local stress and strain fields in the stressed material further complicate the matter. This speaks in favour of selecting a relatively simple model for coupling micro- and macro-mechanics of the FRC composites. The force transmitted by the fibres that bridge the free surfaces of a sub-macrocrack, is built up with the components of the fibre forces perpendicularly to the crack plane. The crack opening displacement behaviour will therefore be governed by the total projected fibre

length in a normal direction to the crack plane. For the most relevant situation of a partially planar-oriented fibre structure, the average embedment length in the normal direction is given by this author [Stroeven and Shah, 1978]. This expression reduces for a spatial random distribution to $\frac{1}{6}l$, instead of the commonly adopted value $\frac{1}{4}l$, l being the fibre length.

The possibilities for designing on the basis of micromechanical properties can be explored by comparing experimental data of the "same" material on micro- as well as on macroscopical level. This approach has been pursued in the research program reported on. To that end, the following three sub-programs have been executed:

a. pull-out tests on single fibres;
b. tensile tests on relatively large FRC specimens;
c. morphological studies of the fibre structure in the specimens used in the test series of sub b.

Three different fibre types have been taken into consideration throughout all the investigations.

We have previously reported on these three subjects. For more details of the test techniques the reader is therefore referred to these publications [Shah and Stroeven, et al., 1978; Stroeven and Shah, et al., 1978; Stroeven and Shah, 1978].

Further, the results of the three studies are compiled in full detail in Bouter [1979], Stroeven [1980b] and Stroeven and Dalhuisen [1980]. Additional morphological investigations have revealed still more complicated features of the fibre structure as adopted in this publication. Moreover, centre-point static bending tests have been performed to evaluate the effect of systematic changes in the fibre morphology on the load-bearing capacity. We will not make use of these results, however, when elaborating the tensile experiments. Information on this subject can be found in Stroeven [1980a] and Donker [1979].

2 Experimental programs and test set-ups

2.1 *Materials variables*

The experiments encompassed three types of fibres and four types of mortar matrices. In all relevant cases we have added to the matrices 1.73 volume percentage of the following fibres*:

a. straight fibres, 25 mm long and 0.39 mm in diameter;
b. fibres with hooks at their ends, 30 mm long and 0.40 mm in diameter;
c. fibres with paddles at their ends, 50 mm long and 0.75 mm in diameter.

The matrix variables included the water to cement ratio (wc) and the fineness modulus $(f_i) \cdot$ wc and f_i has been given the following values in the case of the
- pull-out experiments: wc = 0.40 and 0.60; f_i = 3.27 and 3.89;
- tensile experiments: wc = 0.35 and 0.45; f_i = 3.27 and 3.89.

A Portland Cement type A was used. The sand had a maximum grain size of 8 mm. The

* viz. Appendix A1.

8

Table 1. Mix design according to DIN 4188 and DIN 4187.

$f_i = 3.27$			$f_i = 3.89$		
sieve opening	sieve rest		sieve opening	sieve rest	
mm	%	kg	mm	%	kg
4–8	15	0.750	4–8	26	1.300
2–4	14	0.700	2–4	17	0.850
1–2	14	0.700	1–2	15	0.750
0.5–1.0	18	0.900	0.5–1.0	15	0.750
0.25–0.5	18	0.900	0.25–0.5	16	0.800
0.1–0.25	21	1.050	0.1–0.25	11	0.550
	100	5.000		100	5.000

PC type A 2000 gram $\}$ wc = 0.4	PC type A 2000 gram $\}$ wc = 0.6
Water 800 gram	Water 1200 gram

sand to cement ratio by weight amounted to 2.5. The aggregate grading is shown in Table 1.

2.2 Pull-out experiments

Small prismatic specimens $(40 \times 40 \times 160$ mm$)$, all containing a centrically embedded fibre and a pre-existing crack, were subjected to monotonically increasing deformations in an Instron-testing machine (Fig. 1). The rate of cross-head movement was kept at 2
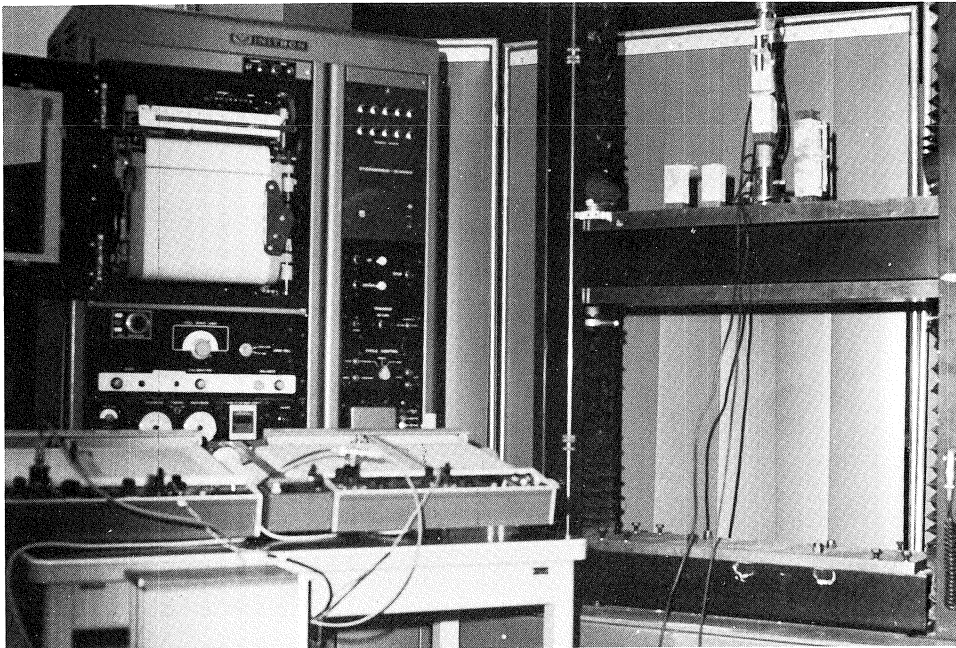

Fig. 1. Testing arrangement for the pull-out experiments.

mm per minute. Relative displacements were recorded between the specimens halves, and between the plastic plate and these halves. Since no displacement was recorded between the plastic plate and the part of the specimen containing the anchored end of the fibre, and it was proven that no eccentricity occurred during testing, the results could solely be based upon a single continuous recording of relative displacements between both specimen halves. The recording was accomplished with the help of inductive divices (Fig. 2).

The tensile loading was introduced in the specimen by means of steel bars screwed into steel plates that were glued to the specimen ends. During handling of the specimens, the specimen halves were connected by a steel strip to avoid relative displace-
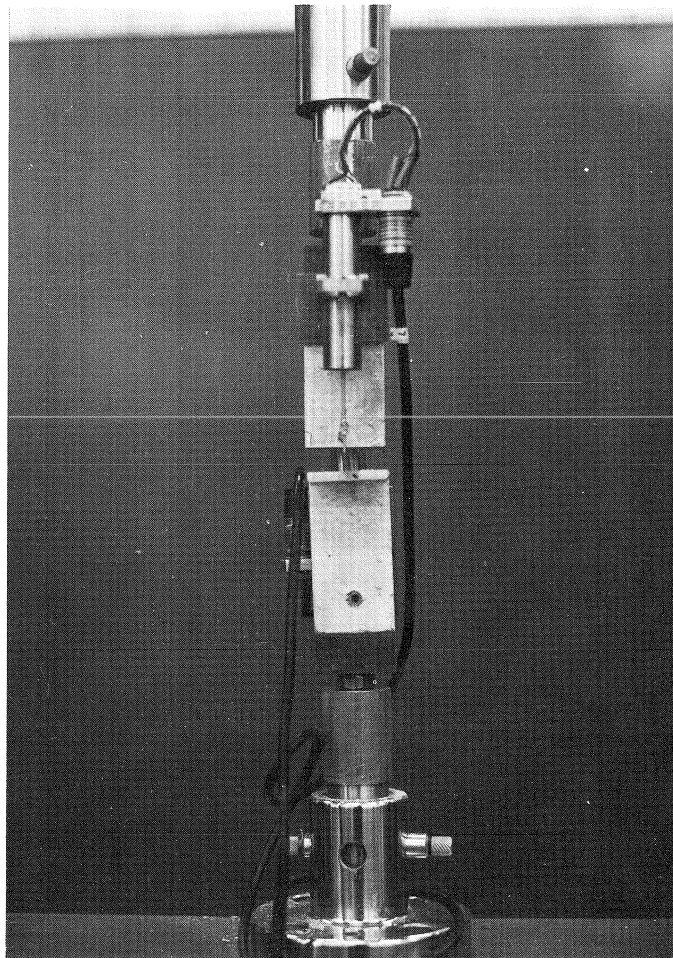

Fig. 2.   Detail of the mortar specimen in the Instron testing machine at termination of the pull-out test.

10

ments and, hence, damage to the fibre matrix interface (Fig. 3).The applied loading was recorded by a load cell.

The specimens were tested at 28 days after storage under water up to a few hours before testing. To improve the reliability of the group average values, a test was repeated six times. For more details of the testing procedure see Stroeven and Shah, et al., [1978]. As can be observed, the described procedure combines some of the advantages of the different approaches in vogue [Burakiewicz, 1977; Hughes and Fattuhi, 1975; Maage, 1976]. The investigations were intended to be continued on groups of parallel fibres with an average spacing corresponding to the one met in the tensile test. However, the hooked and paddled fibres exerted such an improved load-bearing capacity as compared to the conventional straight fibres, that in an early state of loading the mortar specimens were disruptured. This is in itself a striking observation, reflecting the superiority in load transfer capability and toughness of these fibre composites as compared to the composites containing the straight fibres.

2.3   Uniaxial tension tests

Large specimens (50 × 200 × 1000 mm) have been applied in the tensile experiments. They were subjected to uniaxial tension in a 600 kN servo-hydraulic testing machine
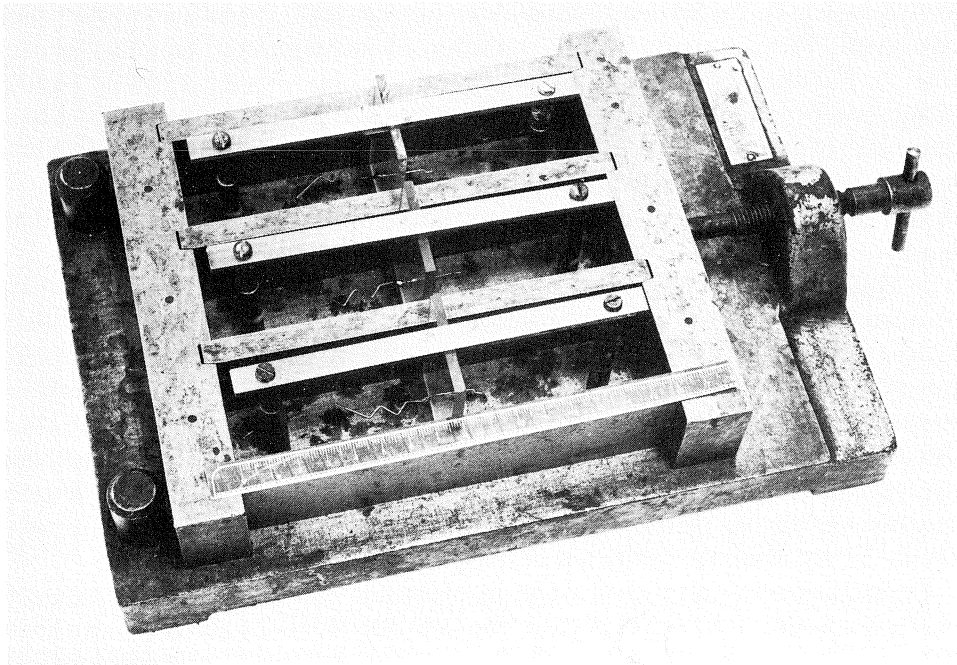

Fig. 3.   Mould for the pull-out specimens prior to filling up with the mortar.
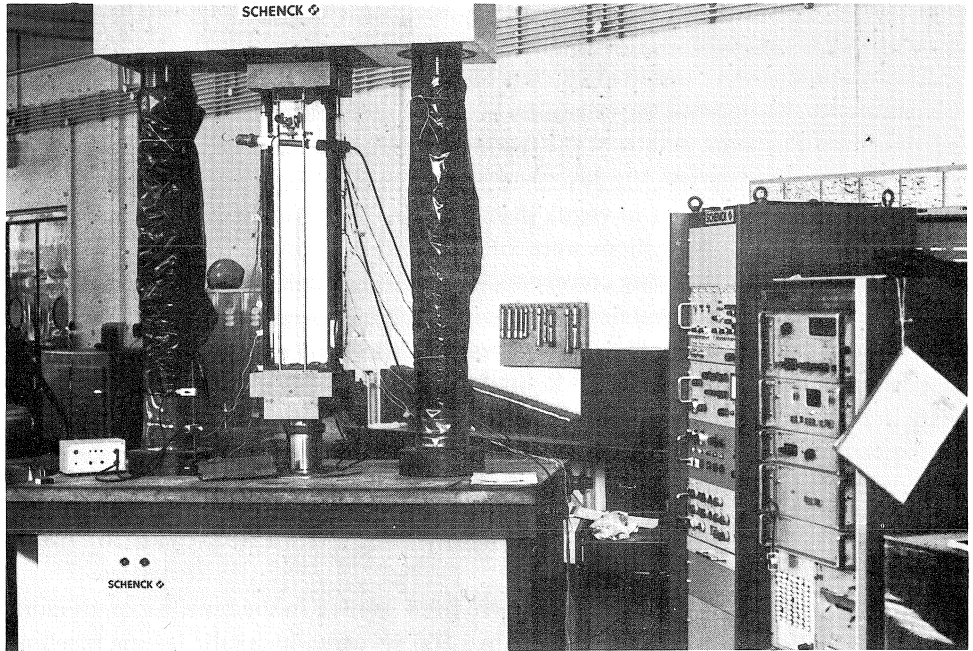
Fig. 4.   Testing arrangement for the direct tension experiments.

(Schenck) (Fig. 4). The apparatus was stiffened by means of four steel bars loaded paral-
lel with the FRC specimen, to facilitate recording of the complete stress-strain diagrams
(Fig. 5). The design provided for increase in total loading over the complete loading
range, despite structural loosening of the concrete specimen. The load was stepwise
increased (15 kN per minute) up to a total loading of 600 kN, the load increments being
4.8 kN to a stage where the specimen revealed an ever decreasing stiffness, whereupon
the load increment was doubled. A single test lasted, as a result, between two and three
hours.

   In longitudinal direction the specimen has been provided with 7 strain gauge trans-
ducers at each side. Further, strain gauges have been fixed to the four calibrated stiffen-
ing bars. In doing so, the phenomenological behaviour of the specimen could be estab-
lished by subtracting the load-deformation characteristics of the stiffening bars from
that of the complete system. The relative inaccuracy in such an increment of two large
values is an inherent disadvantage of the selected test arrangement. Measurements of
the crack opening were accomplished by means of a travelling microscope with an
accuracy of 0.02 mm, mounted in front of the specimen. The crack opening has only
been recorded along the centre line at the front side of the specimen.

   The specimens were fabricated in horizontal position, stored in a water tank until the
day before testing at an age of 28 days. The steel platens were glued to the specimen
ends with an epoxy. The epoxy was permitted to cure under relatively low compressive
stresses in the testing machine for about 24 hours. To avoid failure at the specimen

12

ends, the epoxy was smeared out over a couple of centimeters along the roughened outer surfaces of the specimen.

Data representative for stresses and strains were fed into a 200 channel data-acquisition system (DY 2010 D-HP). The data were recorded on a print-out tape as well as on a computer tape. This latter facility offered the opportunity for computer (HP 21 MX) manipulations with the results. Apart from the stress-strain curves reflecting the real mechanical behaviour manifested at 14 different places along the specimens, the computer produced approximated stress strain curves. This approximation was aimed at "smoothing" the irregularities in the curve. This was accomplished by linear regression approximations of the ascending as well as descending branches of the stress-strain curves.

To improve the reliability of the group averages, all tests were repeated three times. Plain mortar specimens included the program encompassed $3 \times 2(wc) \times 2(f_i) \times 4$(fibre type, plain m.) $= 48$ specimens.

Since some specimens failed inside the areas extended over 50 mm at both specimen ends and not covered by strain gauge transducers, group averages are sometimes based
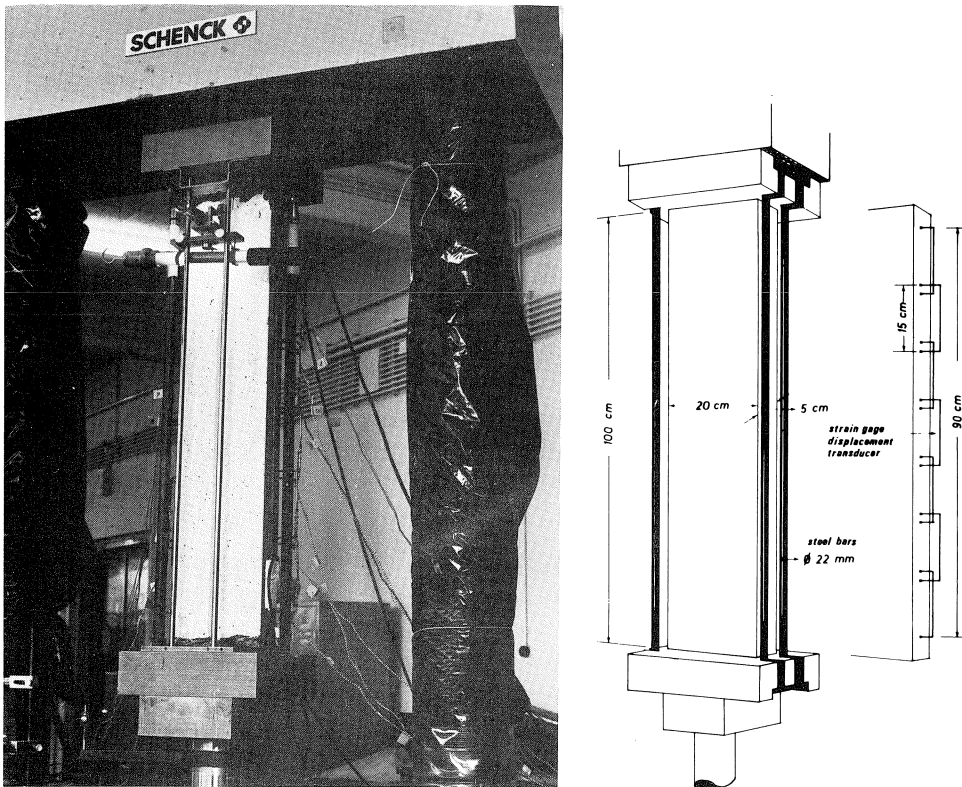

Fig. 5. View of specimen, parallel stiffening bars and mounted strain gauge transducers and travelling microscope.

13

on less than three data. For additional details of the experimental set-up the reader is referred to Shah and Stroeven, et al., [1978]. A similar approach for obtaining complete stress-strain diagrams for plain concrete was previously applied by Hughes and Chapman [1965].

2.4 *Morphological study*

For a morphological analysis of the actual features of the fibre structure, the specimens were sawed into 11 parts of about equal size. By removing a slice with a thickness of approximately 10 mm from these parts, a series of 10 parallel and nearly equidistant slices, evenly distributed along the specimen length, was obtained (Fig. 6). These slices were subjected to two different quantitative image analysis techniques, i.e. X-ray radiography-image analysis and feature (fibre intersection) counting. The first technique required the preparations of X-ray radiographs, which was accomplished with a Radiofluor 360 unit manufactured by Torr X-ray Corp. Good contrast radiographs were obtained under radiation with 80 kV, 3 mA and 35 seconds exposure time [see, e.g. Kasperkiewicz, et al., 1978].
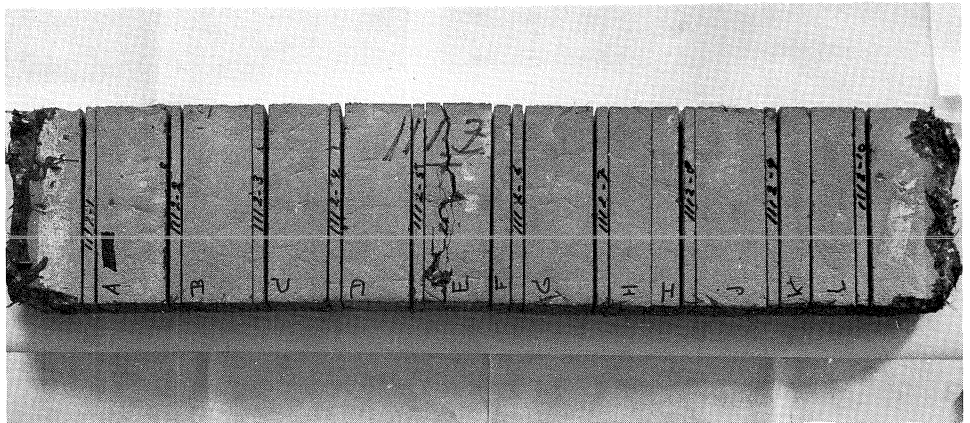
Fig. 6.　Arrangement of the slices applied for X-ray radiography image analysis along the length of a specimen.

These projection images of the fibre parts (included in the slice) were analysed by superimposing a line grid in two successive orthogonal positions and counting the number of intersections. For the paddled fibre type FRC specimens, a total grid line length of 900 mm was used, while in the other two cases a test line with a length of 360 mm was applied. This approach provided information with respect to local density as well as to direction and degree of preferred orientation. For the theoretical background (based on geometrical probability theory) one is referred to previous publications of this author [Stroeven, 1977 and 1979]. The alternative approach of counting fibre sections was planned to check the above-mentioned results. Calculation of the fibre efficiency, more-

14

over, requires additional information with respect to the spatial dispersion of these fibres that can only be obtained from the radiographs. A total number of 360 projection images, and alternatively, sections, has been analysed by these two techniques. More extensive information can be obtained from Stroeven and Shah [1978]. Additional morphometrical investigations of elements oriented in the axial direction of the specimen revealed more complicated morphological features than the one used to construct the structural model on which the evaluation of the macromechanical results is based. Part of this latter information is compiled in Donker [1979] and Stroeven [1980a]. We shall only refer to these morphological features in the discussion of the results.

3 Results

3.1 *Pull-out experiments*

The primary results are the load-displacement diagrams. Some representative examples covering the three fibre types investigated are combined in Fig. 7, so that characteristic features can directly be compared. Notwithstanding the differences in embedded surface area, these curves already reveal the improvement of the load-bearing capacity by hooks and paddles.

Three domains can be distinguished in the pull-out behaviour. Up to the limit of proportionality (LOP) the ascending branch of the load-displacement curve is a straight line. The last part of the curve can be approximated by a straight line, $P = b_1 + b_2 \cdot w$, gradually descending from the maximum post cracking strength (MPCS) in the case of
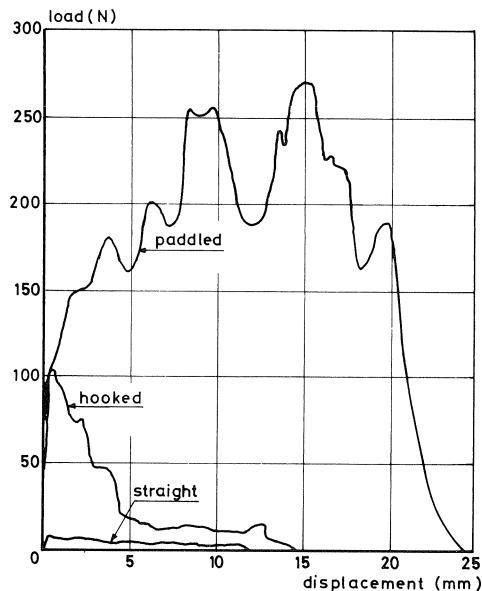
Fig. 7. Typical load-displacement curves for the three types of fibres encompassed in the pullout experiments.

15

the hooked and straight fibres, and indicating a constant load in the case of the paddled fibres, $P_{max} = b_1$. w is the crack opening (pull-out distance), b_1 is the load intercept and b_2 the regression coefficient of the regression line of P on w. This approach facilitates easy calculation of the dynamic friction resistance, τ_f, under the assumption of a uniform stress distribution along the embedded fibre length. It can be shown that

$$\tau_f = \frac{b_2}{\pi d} \qquad \text{(straight and hooked fibres)} \qquad (1a)$$

$$\tau_f = \frac{2b_1}{\pi d l} \qquad \text{(paddled fibres)} \qquad (1b)$$

In the latter case the constant resistance can only be due to the "ploughing" action of the paddle. The actual maximum stresses will, therefore, considerably exceed those calculated by eq. (1b). The initially linear reduction of the load for the smooth and hooked fibres is due to the gradually deminishing embedment length.

The shear strength, τ_a, could be derived from the LOP, assuming a triangular interfacial shear stress distribution. Hence

$$\tau_a = \frac{4 \cdot \text{LOP}}{\pi d l} \qquad (2)$$

Unfortunately, it was not possible to locate the LOP accurately enough for the straight fibres. The results, as a consequence, show an enormous scatter, as could be expected for such an extremely structure-sensitive property. In between LOP and MPCS, the three fibre types manifest different characteristics. For the straight fibres the range between LOP and ultimate tensile strength (UTS) varies widely, as was previously also found by Den Boer [1973]. The origin for the occurrence of a UTS varying between values well exceeding the MPCS and the MPCS itself can be found in the screwdriver-shaped fibre ends (Fig. 8). Because of the width variations, the ploughing action of the fibre ends will fluctuate strongly. Pinchin [1977] has already directed the attention to this effect. This contribution to the load-bearing capacity has probably also improved the deformability at the ultimate load. An average crack opening of 2.8 mm is found!

In the case of the hooked fibres, the intermediate part of the load-deformation curve always has a pronounced top (UTS). The first part of the descending branch reveals two threshold values for the load, reflecting modifications in the geometry of the hook. The crack opening at ultimate loading is 0.62 mm. Thé LOP is, on the average, situated at 31.4% of the UTS value. In the case of the paddled fibres, the intermediate part of the load-displacement curve constitutes a gradual bend over from the linear ascending branch, terminating in the LOP towards the last, approximately horizontal part of the curve (equalling the MPCS). A peak loading can either be attained during the intermediate or even the last part of the loading range. This causes difficulties in defining the maximum stable crack size. Quite large values have, nevertheless, been recorded. The high contribution of the paddle in transferring the load from the fibre to the matrix has improved the range between LOP and UTS. The LOP is, on the average, situated at 21.2% of the UTS value.

16

It was confirmed by the experiments that the LOP, UTS and MPCS values were successively less influenced by differences in the water to cement ratio. The maximum shear strength, τ_{max}, and the dynamic friction resistance, τ_f, represented in graphical form as functions of wc and f_i in Fig. 9, may serve to demonstrate this.

Roughly speaking, one can conclude that for the straight fibres the water to cement ratio more dominantly influenced the ultimate strength and hence the maximum shear strength, while the fineness modulus had a more pronounced effect on the dynamic friction resistance. However, the hook, and even stronger, the paddle, make an additional appeal to the compressive strength of the matrix. As a result, a considerable increase in both strength parameters is attained for the paddled fibres when reducing the water to cement ratio, while a moderate gain is achieved by raising the fineness modulus. Table 2 contains some additional contracted data.
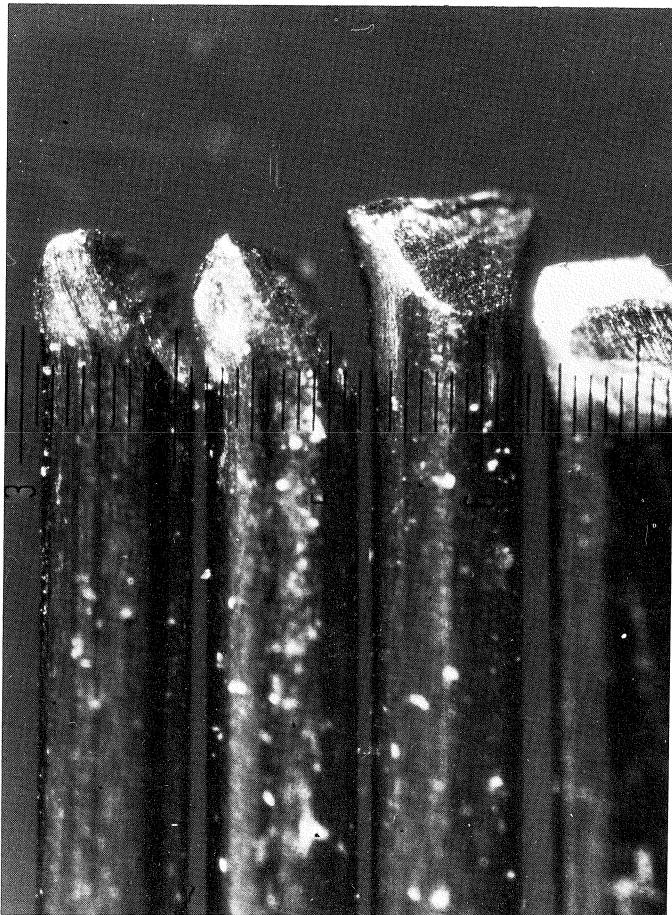

Fig. 8.   Magnification of the straight fibres used in the investigations, revealing the screwdriver fibre ends.
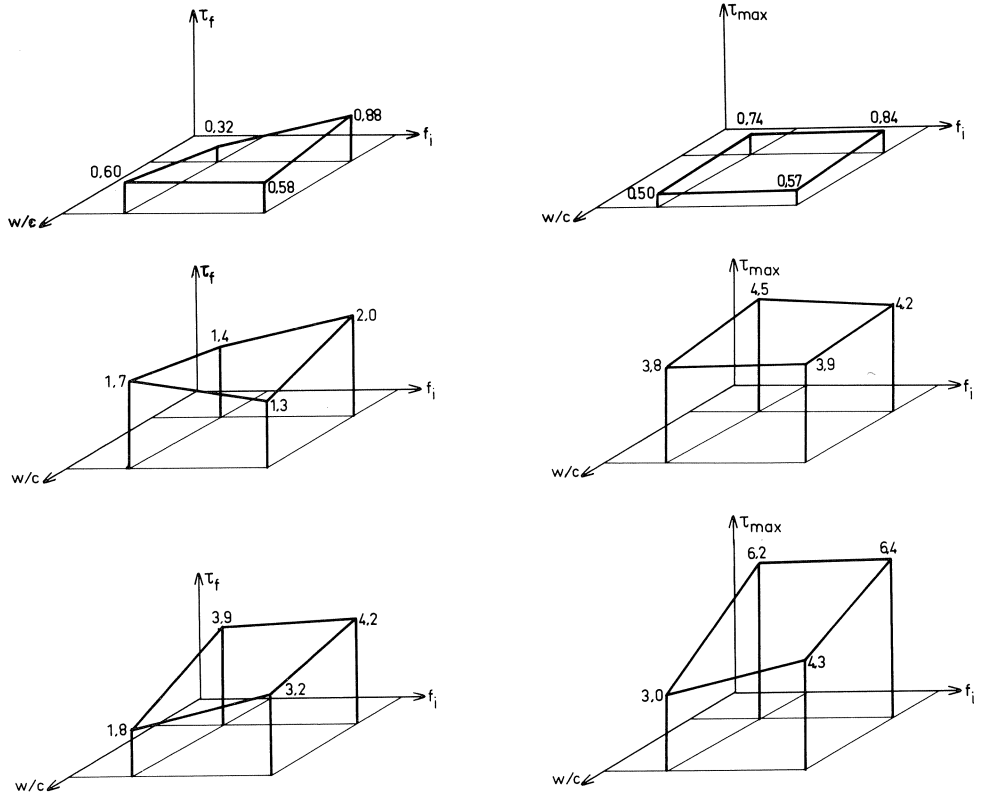
Fig. 9. Dynamic friction resistance, τ_f, and maximum shear strength, τ_{max}, both as a function of fibre type, water to cement ratio and fineness modulus. From top to bottom: straight, hooked and paddled fibres, respectively. Results in N/mm^2.

Table 2. Mechanical properties of three types of fibres in pull-out experiments. Apart from average properties it presents the sample size, n, and the coefficient of variation, cv.

fibre type	wc	f_i	n	P_u	cv	n	P_a	cv	n	τ_f	cv	n	δ_{pu}	cv	n	G	cv
	–	–	–	N	%	–	N	%	–	N/mm^2	%	–	mm	%	–	N·mm	%
hooked	0.4	3.89	6	82	13	4	12	78	6	2.0	48	6	0.6	27	5	226	39
	0.6	3.89	6	76	18	6	38	55	6	1.3	24	6	0.7	15	6	259	19
	0.4	3.27	6	87	17	4	32	48	6	1.4	73	5	0.6	50	5	307	29
	0.6	3.27	6	74	9	6	18	144	6	1.7	23	6	0.6	33	6	293	14
straight	0.4	3.89	6	12	39	–	–	–	6	0.9	47	6	1.6	71	6	78	40
	0.6	3.89	6	8	47	–	–	–	6	0.5	62	6	1.2	193	6	47	71
	0.4	3.27	6	11	95	–	–	–	6	0.3	78	6	3.7	100	6	31	99
	0.6	3.27	6	7	62	–	–	–	6	0.6	55	6	4.7	72	6	40	58
paddled	0.4	3.89	6	377	10	4	81	43	4	4.2	36	4	–	–	1	5505	–
	0.6	3.89	6	251	26	4	24	139	4	3.2	20	4	–	–	4	3856	11
	0.4	3.27	6	364	21	3	118	49	3	3.9	37	3	–	–	1	3340	–
	0.6	3.27	6	179	28	5	43	57	5	1.8	11	5	–	–	5	2370	7

18

For more detailed information the reader is referred to Bouter [1979]. An important parameter, additionally, is the dissipated energy per unit of embedded surface area or specific (fracture) toughness, G_s. Due to the ploughing action of the hook, the area under the load-displacement curve of the paddled fibres is by far the largest, as can be seen in Fig. 7. As a result, the specific fracture toughness values are also superior. Hence, compared on the basis of unit embedded surface area, the paddled fibres combine favourable load-bearing capacity with high toughness values. The straight fibres are obviously the least effective.

3.2 Uniaxial tension tests

Primary results are in this case the stress-strain curves of the successive sections of a specimen and the microscopical observations of crack growth along the front centre line. For a first indication of differences in mechanical behaviour due to the distinct fibre types, however, we may attach a higher value to the modified diagrams. A representative set is presented in Fig. 10.

The extension of the domains I and III have been selected by eye, whereupon the stress-strain data were subjected to a linear regression analysis on the basis of equations of the type

$$\sigma = b_1 + b_2 \varepsilon \tag{3}$$

Young's modulus of the composite, E_c, follows directly from

$$E_c = b_2$$

where b_2 is the regression coefficient of the regression line in domain I. The dynamic friction resistance, τ_f, is, in analogy with the pull-out experiments, given by [Stroeven and Dalhuisen, 1980]

$$\tau_f = \frac{b_2 A}{2\pi d N s} \tag{5}$$

in which b_2 is the regression coefficient of the regression line in domain III, N the number of fibres in the cross-section, d the fibre diameter, s the measuring length of the strain gauge transducers and A the surface area of the cross-section.

A maximum resistance, UTS, is mostly detected between LOP and MPCS values. The UTS value rises beyond the top of the triangle, however, in a deminishing degree from the straight to the hooked and paddled FRC specimen, respectively.

The plain mortar strength results (Fig. 11) reveal a roughly equal influencing of wc and f_i values on the strength results, i.e. about 10% over the measuring ranges. The ratio of splitting tensile to uniaxial tensile strength is 1.66. Fig. 13 shows the fibre contribution to the load-bearing capacity, assuming the contribution of the matrix to be independent on the fibre addition [Hannant, 1978; Aveston, Cooper and Kelly, 1972].

Uniaxial tensile strength and splitting tensile strength data yield consistent results for the fibre contribution to the load-bearing capacity. For the straight, the hooked and the paddled fibre types FRC specimens, respectively, we find, on the average, 24%, 63%

19
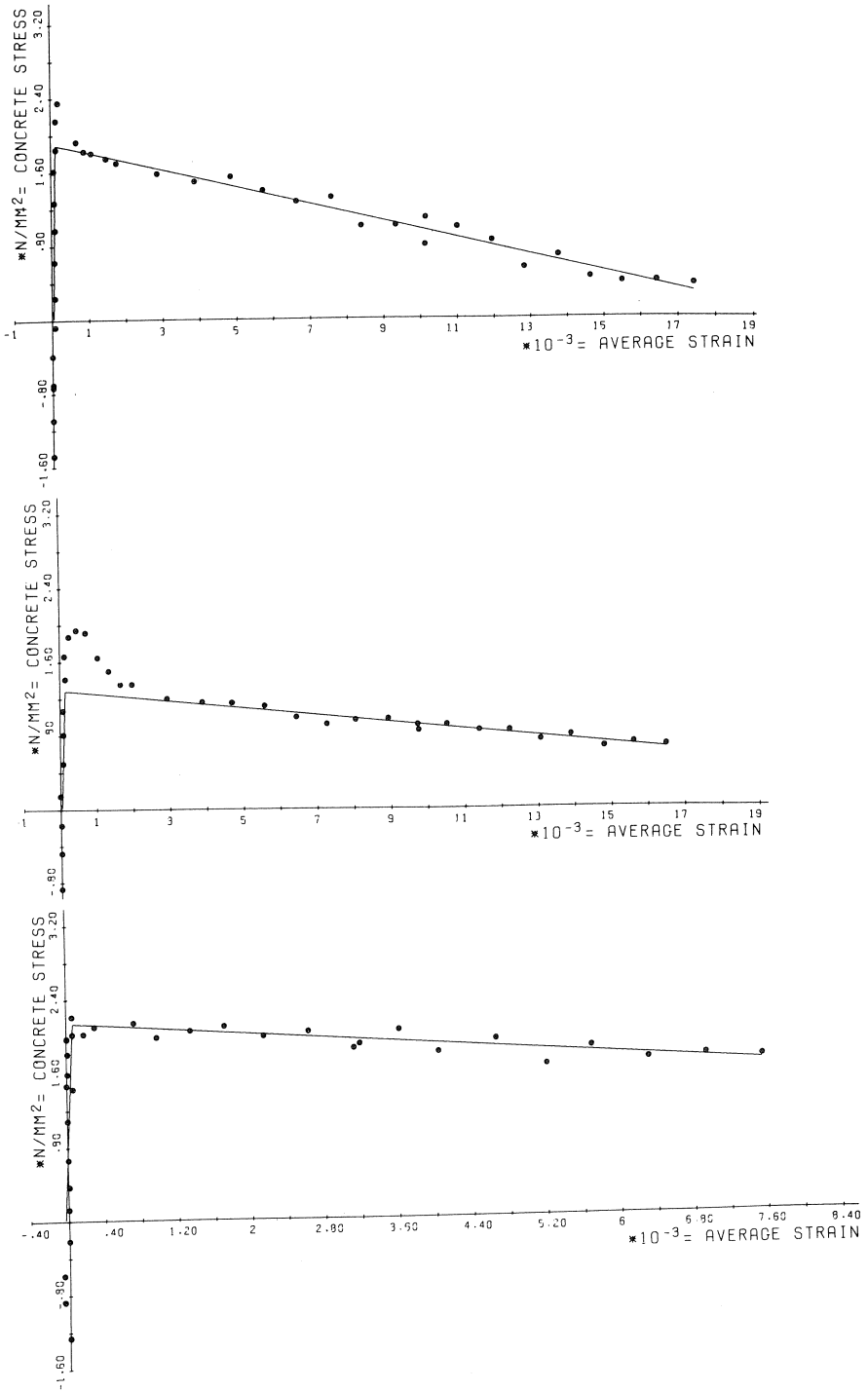
Fig. 10. Typical examples of approximated stress-strain diagrams, from top to bottom representing FRC specimens containing straight, hooked and paddled fibres, respectively.
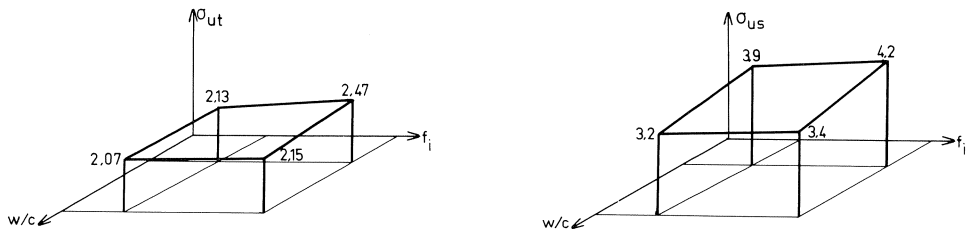
Fig. 11. Direct and splitting tensile strength data of plain mortar. Results (in N/mm² are given as a function of the water to cement ratio and the fineness modulus.
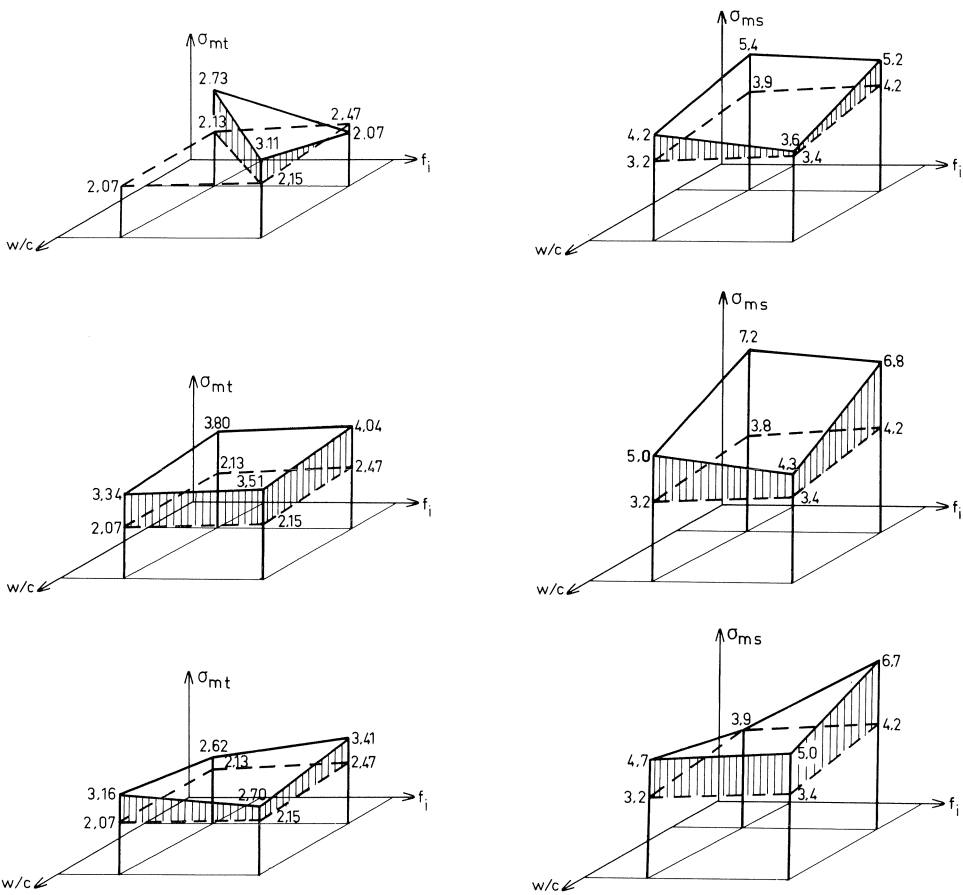

Fig. 12. Fibre contribution to the ultimate tensile strength as revealed in the direct tensile test (at the left) and the Brazilian splitting test (at the right) and shown as a function of the water to cement ratio and the fineness modulus. From top to bottom: straight, hooked and paddled fibres, respectively. Results in N/mm².
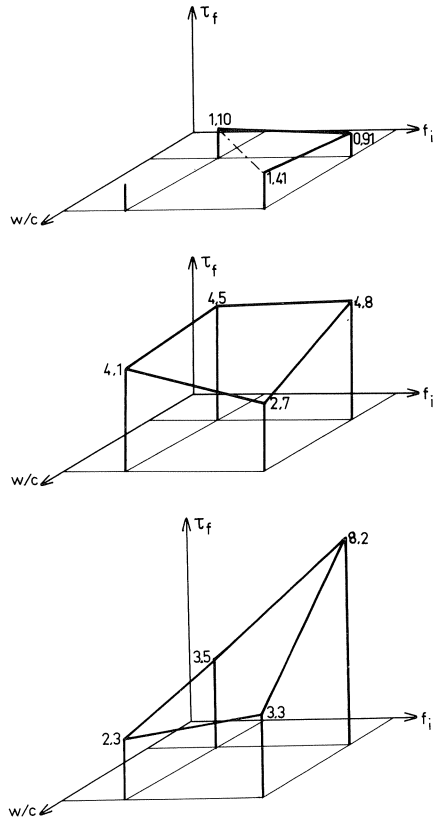
Fig. 13. Dynamic friction resistance, τ_f, as calculated from eq. (5), shown as a function of the water to cement ratio and the fineness modulus. From top to bottom: the straight, the hooked and the paddled fibres, respectively. Results in N/mm².

and 34% strength gain due to the fibre addition. These results fall in the range of relevant data presented in the literature [CUR, 1977; Moens and Nemegeer, 1978; Johnston and Coleman, 1978]. It is worth calling attention to the favourable results of the hooked fibres. Despite a better performance of the paddled fibres in pull-out behaviour (e.g. maximum load-bearing capacity per unit of embedded fibre length), the hooked fibres, smaller in size, and outnumbering the paddled fibres, score considerably better as a group.

The strength results, presented in Fig. 12, show a favourable effect of the water to cement ratio on the fibre contribution to the ultimate strength in uniaxial tension as well as in the splitting tensile test. The fineness modulus cannot be attributed a systematic influence on the composite strength. Notably poor, though, are the results of the paddled fibre type FRC specimens with wc = 0.35 and f_i = 3.27. The dynamic friction resistance is presented in graphical form as a function of wc and f_i in Fig. 13.

In particular the dynamic friction resistance data of the hooked and paddled fibre types FRC specimens reveal an influence of the water to cement ratio. A considerable

leading crack, the additional diagrams reveal interesting characteristics, particularly when viewed in combination with the corresponding crack growth data. A representative set of such diagrams, crack patterns and crack growth data is presented in Figs. 17–19.
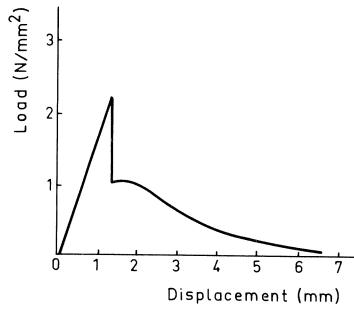

Fig. 15. Typical stress-strain curve for a FRC specimen in tension containing straight fibres.
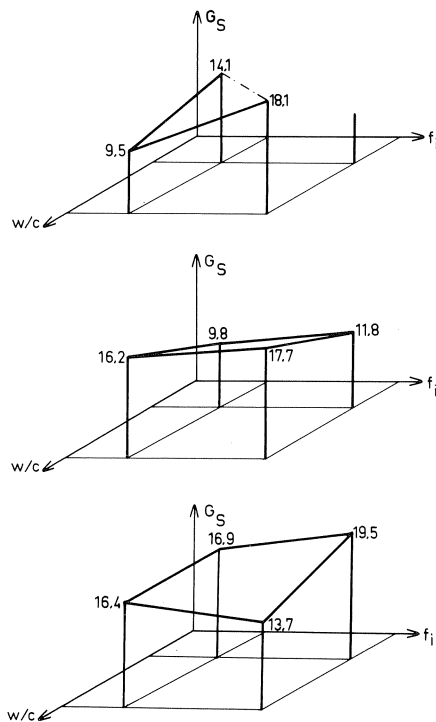

Fig. 16. Specific toughness results for the three fibre types FRC specimens shown as a function of the water to cement ratio and the fineness modulus. From top to bottom: straight, hooked and paddled fibres, respectively. Results in N/mm.

25
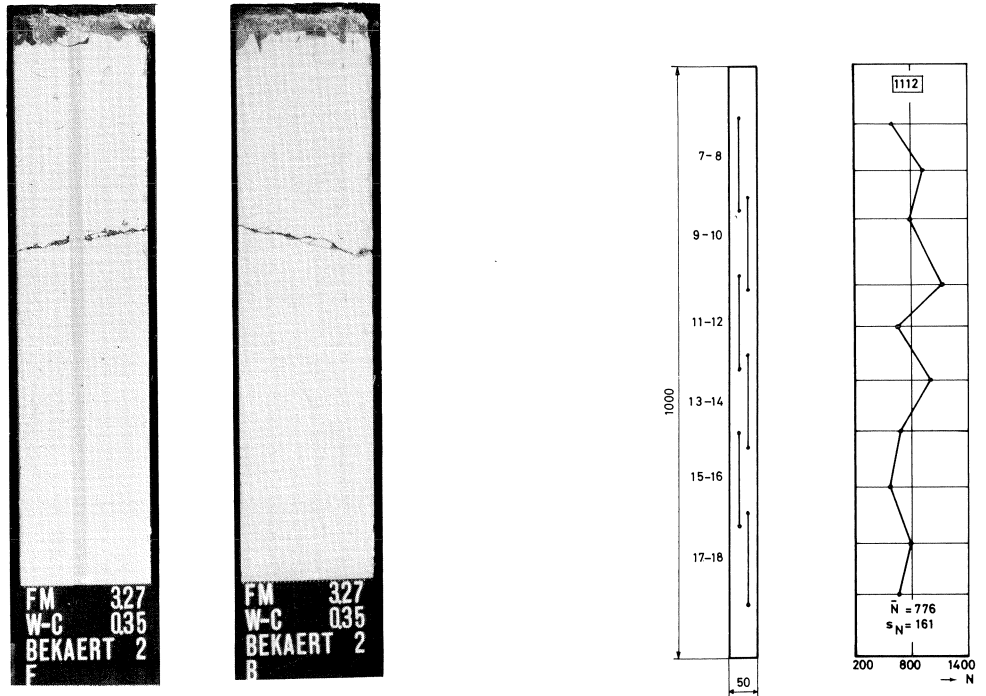
Fig. 17. Example of a FRC specimen containing hooked fibres, previously subjected to direct tension. The crack patterns at front and back side of the specimen are shown at the top left. At the top right are plotted the sequence of strain gauge transducers and the variation along the specimen axis in the number of fibres per unit area of the cross-section. The picture at the bottom presents the crack growth data (measured by the microscope) and (average) deformations recorded by the indicated transducers. The macrocrack was developed in a region where the fibre density is extremely low. Cracks that were successively initiated under rising loads have grown in a proportional way.

26
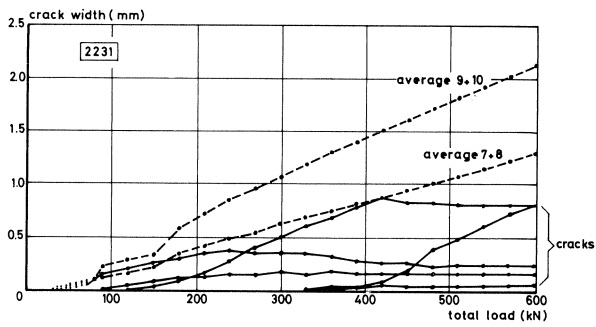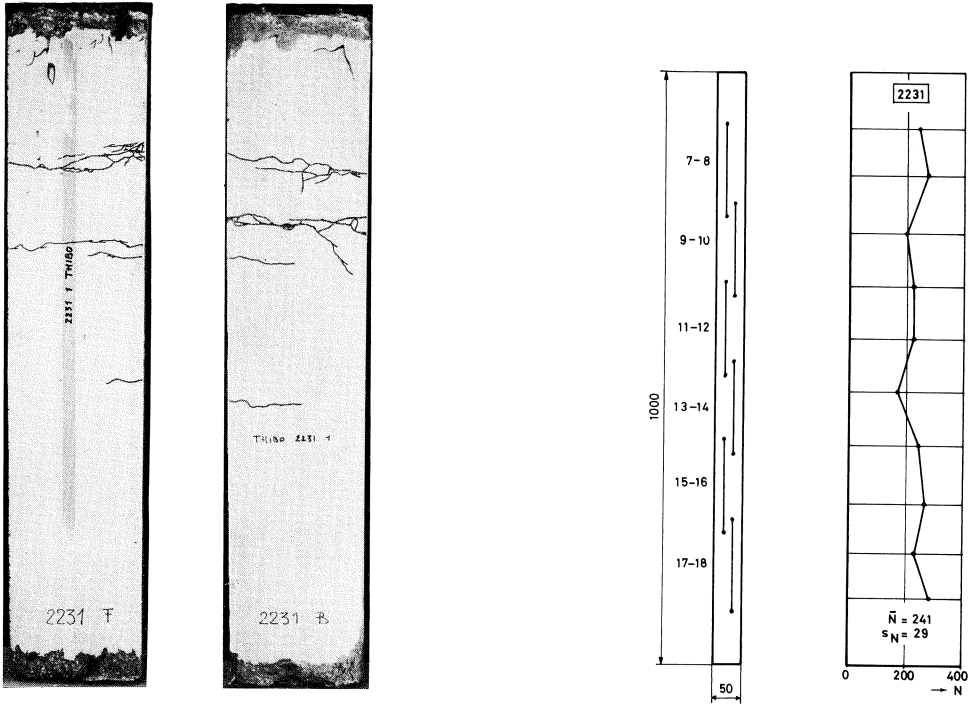
Fig. 18.   Prismatic FRC specimen containing paddled fibres, previously subjected to direct tension. For explanation see Fig. 17.
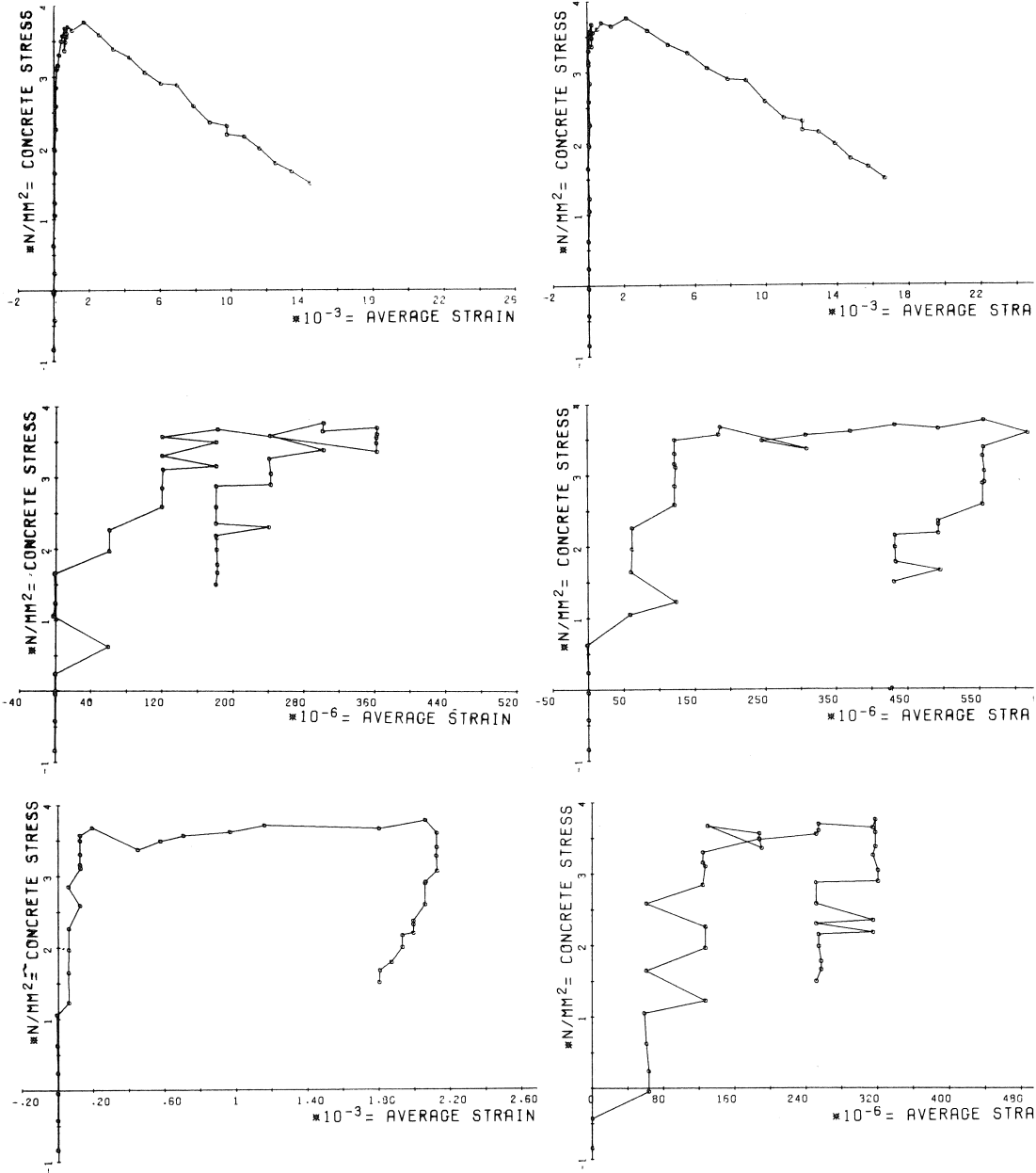
Fig. 19. Examples of stress-strain curves of neighbouring regions (transducers 7 to 12) of a FRC specimen containing hooked fibres. Cracking in the weakest region (at the top) is accompanied by micro- and sub-macrocracking up to various degrees in other regions. Crack initiation takes place at different percentages of ultimate in the different measuring sections. Note that the zero stress level is situated at -0.56 N/mm^2.

28

The following conclusions can be drawn:
- a varying number of the 14 stress-strain diagrams of specimens of all mixes show approximately coinciding ascending and descending branches, whereby the maximum strain attains values up to 120–125 µstrain*;
- a number of stress-strain diagrams of the straight fibre type FRC specimens show strains of about 180 µstrain without visible cracking. In the case of hooked and paddled fibres this value is increased to 250–280 µstrain. Permanent deformations are revealed under reduced loading;
- deformations frequently occur in the range of 400–700 µstrain in the hooked and paddled fibre types FRC specimens. These cracks are detected by the microscope. Upon load release, part of the deformations is recovered. However, the descending branch is less steep as compared to the ascending one (hence, we find a reduced Young's modulus);
- The same specimens, in particular the hooked fibre ones, show stabilizing cracks up to 1.5 mm (corresponding to about 9000 µstrain);
- with the hooked fibre type FRC specimens, cracking can take place at one side of the specimen, while at the other side the material contracts. This seldom occurs with the paddled fibre type FRC specimens;
- in the process of multiple cracking (on the visible level) the leading crack can have either position in the sequence of successively developing cracks;
- crack "initiation" takes place at different fractions of ultimate in the various sections of the specimens;
- the stress-strain curves of the section containing the leading crack mostly show two peaks. In the other sections where cracking occurs, these cracks grow in this domain under nearly constant loading. Particularly for the straight fibre type FRC specimens this traject of yielding is very short;
- the average number of macrocracks (over 1000 mm length) increases from the straight (1.2 per m) to the hooked (1.6 per m) and paddled (2.5 per m) fibre type FRC specimens;
- sub-macro crack intensity in the separate cracked regions seems roughly similar for the hooked and paddled fibre types FRC specimens. It is, however, much higher than in the case of the straight fibre type FRC specimens;
- even for the hooked fibre type FRC specimens** the average opening of the leading crack at maximum loading, i.e. 0.113 mm (corresponding to 720 µstrain) is relatively small. The size of this crack in itself is not an indication that this will become the leading crack;
- Aveston and Kelly [1973] propose formulae for the calculation of micro crack spacing in FRC composites. Spacing is here a fraction of the fibre length. The average strain is

* multiplied by an overall value of Young's modulus, i.e. 18 kN/mm^2 we find a value of 2.2 N/mm^2, corresponding to the tensile strength of the plain mortar. Further, 1 µstrain = 10^{-6}.

** the hooked fibres revealed the smallest crack opening at maximum loading in the pull-out tests. However, this value was still five times in excess of a similar crack size in the tensile test.

thus increased up to $\bar{\varepsilon} = \frac{1}{2}\varepsilon_u(1 + \alpha)$, with $\alpha = (E_m V_m)/(E_f V_f) \simeq 6$. For $\varepsilon_u = 120$ µstrain we find $\bar{\varepsilon} = 420$ µstrain. As mentioned, this is indeed a strain value frequently occurring for the hooked and paddled fibre types FRC specimens.

3.3 Morphometry of the fibre structure

Three subjects of interest can be distinguished:

a. experimental evaluation of the actual parameters of the fibre structure, assuming a partially planar orientation of the fibres;

b. determination of the morphological parameters of the subset of fibres intersecting a crack plane. The results of sub a can be used to refine the solution for a spatially random system;

c. determination of the solution of sub b for successive sections of the tensile specimens.

For the solution of sub a the fibres are assumed to be disposed in two sub-sets, a spatially random (isometric) one, and a planar portion. This model was proven to be a suitable approximation in previous experiments [Stroeven, 1977; 1978; 1979]. The lineal fractions of both portions are the unknown parameters (i.e. $L_{v_{is}}$ and $L_{v_{pl}}$). The degree of orientation, ω, is defined as

$$\omega = \frac{L_{v_{or}}}{L_{v_{is}} + L_{v_{or}}} \qquad (9)$$

The analyses have revealed an increasing degree of compaction-induced segregation and accompanying anisometry of the fibre structure from the straight to the hooked and the paddled fibre types FRC specimens. Such effects are also mentioned by other investigators [see, e.g. Shah and Rangan, 1971]. Details are given in Stroeven [1980b], Donker [1979]. This effect is due to the different weights of the fibres (23 mg, 30 mg, and 192 mg, respectively).

Fibre density differences between bottom and top halves of the specimens have been found to be as large as 100%. Differences in corresponding ω values are smaller*. Average values for ω are presented in Table 3. Similar measurements performed in orthogonal sections, however, have revealed that serious deviations occur from the partially planar model. It was shown [Stroeven, 1980a] that a linear portion with fibres parallel to the main axis of the specimen had to be added. By combining X-ray radiography-image analysis results and feature count data in sections, the results in Table 4

Table 3.   Degree of orientation of fibres in mortar specimens.

Fibre type	weight mg	ω %	number of samples (about $11 \times 50 \times 200$ mm^3)
straight	23	42.6	50
hooked	30	43.6	20
paddled	192	60.0	30

* viz. Appendix A2.

30

Table 4. Composition of the fibre structures composed of straight or paddled fibres. The hooked fibres score in between.

Fibre type	Composition in % of L_v		
	$L_{v_{lin}}$	$L_{v_{pl}}$	$L_{v_{is}}$
paddled	13	40	47
straight	10	43	47

were obtained. The relative efficiency factors of the successive portions in Table 4 are 1, $2/\pi$ and $\frac{1}{2}$. The results are based on a randomly selected sample.

Morphological considerations clearly demonstrate that even in a spatially random fibre dispersion, the fibres intersecting the crack are far from randomly distributed. In fact the fibre orientation varies as $\sin 2\Theta$, Θ being the angle between the fibre and the loading direction. This demonstrates that the micromechanics of a fibre pulling-out under 45° from the matrix have to be attributed a higher relevance than from those orientated in the loading direction. In a more thorough study than pursued here, we should give special attention to this fact. The average embedment length in the loading direction for partially planar-oriented fibres is given by Stroeven and Shah [1978],

$$l_i = \tfrac{1}{6}l \, \frac{1 + 0.5\omega}{1 + 0.273\omega} \tag{10}$$

which reduces to $l_i = \tfrac{1}{6}l$ for a spatially random system intersected by a (crack) plane. For an average value of $\omega = 0.5$ the embedment length increases up to $l_i = 0.183 \, l$. By accounting for 10% of linearly oriented fibres, again an improvement is attained. We find $l_i = 0.190 \, l$, which is 38% exceeding the value for a random structure, demonstrating the importance of structural investigations.

When the resistance in pull-out testing increases such that the resulting force perpendicular to the crack plane stays constant [viz. test results of Naaman and Shah, 1975], the factor $\frac{1}{6}$ in eq. (10) should be substituted by $\frac{1}{4}$.

Due to the deviations from the partially planar-oriented structure, we have used the feature count results for determining the fluctuations in N_A over the specimen height. Figs. 17–19 show some of the results. The following additional conclusions can be drawn from these figures:

- the gross average number of fibres per section, i.e. 879 for the straight, 869 for the hooked and 254 for the paddled fibre types FRC specimens, are systematically higher than the design values. For a spatially random system (or a partially planar-oriented system, with $\omega = 0.5$) we find for the same types of specimens 762 (810), 688 (772) and 172 (228), respectively. In previous calculations we have used the counted averages;
- the experimental values for the coefficient of variation of the number of fibres for the same sequence of the three types of FRC specimens, i.e. 12.8%, 13.1% and 18.5%, respectively, facilitate determination of the weakest chain links. The crack development results do not present any supporting evidence for such an approach, however, since

31

the leading crack can develop at almost any stage of the process of structural desintegration [see also Swamy and Stavrides, 1975];

- cracking is, nevertheless, roughly localized in those areas where the number of fibres per unit area of the cross-section is a minimum. Particularly in the case of the paddled and hooked fibre types FRC specimens we see also cracks deviating from the transverse direction. Connection of crack location with the graph for N_A over the specimen height is in that case very difficult [viz. also Stroeven and Shah, 1978];
- when a single minimum (or only a couple of distinct minima) occurs in the N_A-curve, the specimen will fail in this (these) section(s). A more even distribution of the fibres along the specimen length favours, however, the development of more macrocracks.

4   Discussion

In comparing the individual and group behaviour manifested in the pull-out and tensile tests, respectively, we see remarkable differences in the stress-strain curves. The matrix, however, has produced a major contribution to the load-bearing capacity of the composite, and as a consequence, has suppressed the differences in the fibre contributions to the strength of the specimens. Spreading the estimated fibre contributions uniformly along the fibre length yields values for the maximum shear resistance, the averages of which are collected in Table 5. These mean values correspond satisfactorily with the corresponding strength values revealed in the pull-out tests.

Table 5.   Values for the maximum shear resistance of individuals and of groups of fibres.

Fibre type	τ_{max} (N/mm^2)	
	individuals	group
straight	0.7	0.8
hooked	4.1	3.5
paddled	5.0	2.1

Only the paddled fibres score on the low side. This is doubtlessly due to the uneven distribution of the large fibres with respect to location and orientation in longitudinal as well as in transverse direction in particular. The origins for strength differences in individual and group test results can be found in the scatter in the strength results (coefficient of variation varies up to a maximum of about 20%), the variation in the number of fibres in a section (with a minimum of about 70% of the average value) and in the crudeness of the stress solution along the fibre length (uniform, or alternatively, with a dowel and/or ploughing load as sketched in Fig. 20). The dynamic friction resistance data produced in the micro- and macromechanical tests reveal differences as can be seen in Table 6.

The arguments presented heretofore also hold in this case. Since τ_f is calculated from the slope of the stress-strain curve, an additional unknown factor is the change in the interfacial stress distribution during slip. Another effect, hitherto not considered, is that

32

Table 6. Values for the dynamic friction resistance of individuals and of groups of fibres.

| Fibre type | τ_f in (N/mm^2) | |
	individuals	group
straight	0.6	1.1
hooked	1.6	4.0
paddled	3.3	3.6

the strain recorded generally stems from more than a single crack. This is very pronounced in the case of the hooked and paddled fibre types FRC specimens. This implies that the number of fibres involved in the slip process will be considerably exceeding the average number counted in the successive sections and used for the calculations. It seems, therefore, that the paddled fibres also score unfavourably concerning group behaviour during slip. The explanation is the one previously given for the poor τ_{max} results.

The significant influence of the water to cement ratio and the less important influence of the fineness modulus on the strength characteristics observed in pull-out testing is also reflected by the results of the tensile test. The latter influence, however, is drawn in the structural scatter. The specific toughness results obtained in the tensile tests fall much closer together than could be predicted from individual behaviour. For the hooked fibre type FRC specimens the two tests lead to quite comparable results. The group behaviour of the paddled fibres reflects the previously mentioned unfavourable circumstances. The reason for the favourable toughness data in the case of the straight fibre type FRC specimens is the incorrect extrapolation due to the misalignement of the regression line, illustrated in Fig. 15. Arguments to support this statement are found in the relatively low value of τ_f (i.e. 0.6 N/mm^2) and the high value of the fictive embedment length derived from the intersection of the regression line and the horizontal axis of the stress-strain diagram (i.e. $l^* = 0.41$ $l \gg l^*_{min} = 0.15$ l). Of course the number of separate sub-macro cracks involved is also a complicating factor, up till now not accounted for. For the rest, a considerable amount of energy is also dissipated in sections not containing the leading crack.

A more thorough evaluation will be pursued in the near future. A sophisticated model must be developed from the results of the structural analyses. The assumed stress distribution (Fig. 20) may have to be modified, too. Up till now we have related S_1 to S_2 by assuming their sum to yield a constant component perpendicular to the crack plane. This facilitated calculation of τ_f from the group behaviour. Since we have used the slope of the regression line for the calculation, we could eliminate S_3 (S_3 does not change its value during the first millimeters of slip). On the other hand, the maximum post cracking strength could be introduced as another source of information. Combination of the data would also facilitate estimating S_3. This makes a comparison with the pull-out test results – where the sum of S_1 and S_3 is measured – more realistic.

Confrontation of the data for paddled fibres in both tests leads to the conclusion, that

for given volume fraction and (maximum) aspect ratio, the selected fibres were inefficiently large. The smaller hooked fibres were therefore more effective in the tensile experiments.

The previously mentioned bending experiments have revealed an analogous mechanical behaviour. In particular, the stress-strain curves measured at the bottom side of the beams show quite similar characteristics as compared to those discussed heretofore. The various amounts of segregation and degrees of anisometry exert their influence in a (not fundamentally) different degree on the mechanical behaviour manifested in both tensile tests. For some data referring to the paddled fibre type FRC specimens, see Appendix A2.
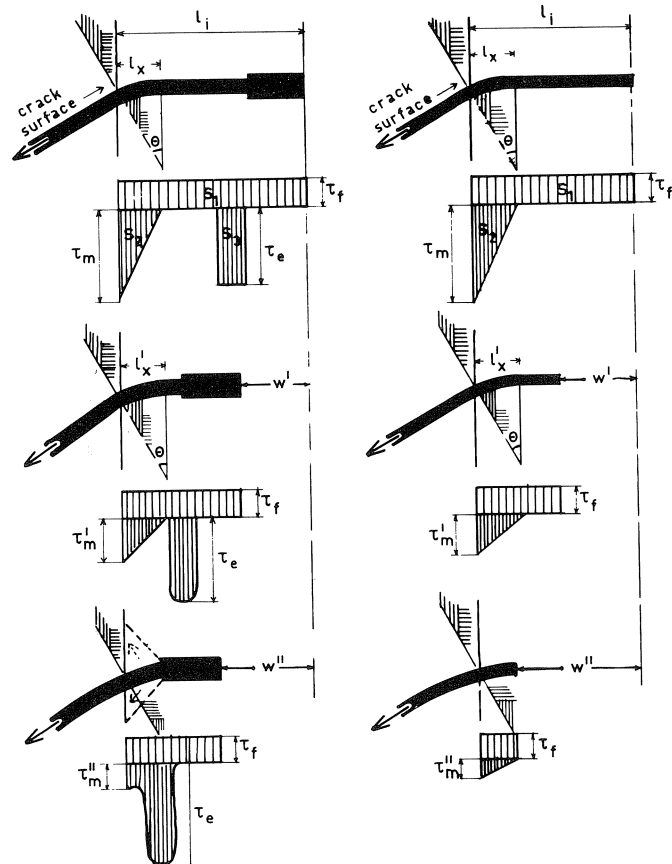

Fig. 20. Geometrical changes occurring during fibre pull-out and the assumed interfacial shear stress distributions.

34

5   Conclusions

Integration of the macro- and micromechanical behaviour, as manifested in the tensile and pull-out test series, can only succesfully be achieved on the basis of the actual morphological features of the fibre structure. The information presented shows that the macromechanical behaviour can be provided with a micromechanical background, although up till now sometimes only of a qualitative nature. Progress can be achieved by more accurately analysing the structural features. A more thorough study of the actual fibre morphology has already been started, as was mentioned before. Another weak link is the lacking knowledge of the stress- strain field in the vicinity of a fibre embedded in a stressed matrix. Only average (continuum mechanical) features (though sometimes incorrectly proposed as local information) can be described by analytical solutions. However, debonding is governed by (local) stress peaks, assuming the bond strength to be uniformly distributed along the interface. In this field we have made some progress by making use of so-called strain nuclei techniques.

The growth characteristics of the crack opening have been shown to depend primarily on the number of fibres involved, the average value of the embedded surface area and the capacity for load transfer in the fibre-matrix interface (viz. Stroeven and Dalhuisen [1980]). We have demonstrated that for fibre dispersions where position and orientation are randomly distributed, the fibres intersected by a plane (crack) are distributed as a $\sin 2\Theta$ function, Θ being the angle enclosed by the fibre and the loading direction. For non-random dispersions one should account for deviations in the orientation distribution. In this publication we have applied the model of a partially planar-oriented structure. Due to values of about 50% for the degree of orientation, usage of this model yields considerable corrections on predictions obtained from a random dispersion model.

What is probably most important is the recognition that micro-mechanical behaviour should be derived from pull-out tests of fibres oriented under, say, 45° with the loading direction. In our approach we have adopted for the straight fibres the relationship $\tau(\Theta) = \tau/\cos\Theta$ for the dependence of the uniformly distributed, interfacial shear stress on the angle enclosed by the fibre and the loading direction. This implies that the load component perpendicular to the crack plane is independent from the orientation of the fibre. This is roughly in agreement with test results of Naaman and Shah [1975].

The composite strength values for the straight low carbon steel fibre types FRC specimens agree satisfactorily with similar results mentioned in the literature, and with a design formula proposed by Naaman and Shah [1975].The composite strength values of the paddled, and particularly of the hooked type of FRC specimens are (much) higher. The hooked fibres have been shown to be the best choice. However, the relatively unfavourable results of the paddled fibre type FRC specimens for strength and toughness, are probably mainly due to the considerable amount of segregation. A smaller fibre (with same volume fraction and aspect ratio) would have scored better. Quite interesting is the correspondence of the toughness data obtained in individual and group tests of the hooked fibres. This implies that only two points of the load-displacement curve are required for a prediction of the toughness, i.e. the maximum post cracking strength

and the average embedment length. In the case of the straight fibres the correspondence was poor. Probably the initial part of the descending branch cannot be used for accurate extrapolation.

It is remarkable that the Brazilian splitting tensile strength results were quite comparable with those of the uniaxial tensile experiments. The percentages strength increase for the three types of FRC specimens fell very close together.

6   References

ARGON, A. S. and W. J. SHACK, (1975). Theories of fibre cement and fibre concrete. RILEM Symp. Fibre reinforced cement and concrete, 14–17 Sept. 1975, London. Construction Press Lancaster, pp. 39–54.

AVESTON, J. and A. KELLY, (1973). Theory of multiple fracture of fibrous composites. J.Mat.Sc., 8, pp. 352–362.

AVESTON, J., G. A. COOPER and A. KELLY, (1972). Single and multiple fracture. Proc. Conf. Properties of fibre composites, Nat. Phys. Lab. Nov. 1971, I.P.C. Science and Technology Press, Guildford, pp. 15–24.

AVESTON, J., R. A. MERCER and J. M. SILLWOOD, (1974). Fibre reinforced cements-Scientific foundations for specifications. Conf. Proc. Composites, standards, testing and design, Nat. Phys. Lab., 8–9 April, 1974. I.P.C. Science and Techn. Press, Guildford, pp. 93–103.

BOER, L. J. DEN (1973). Concrete technology and pull-out testing of steel fibre reinforced normal gravel concrete. Proc. Conf. Properties and applications of fibre reinforced concrete and other fibre reinforced building materials, Sept. 1975, Delft, Univ. Press., pp. 97–106.

BOUTER, C. (1979). Results of pull-out testing of three types of steel fibres embedded in mortar (in Dutch). Stev. Rep. 1-79-3, March, Delft.

BURAKIEWICZ, A. (1977). Bond strength tests for fibre reinforced concrete elements. Proc. First Nat. Conf. Mechanics and technology of composite materials 14–16 Oct. 1976, Varna. Publ. House Bulg. Ac.Sc., Sofia, pp. 771–775.

BURAKIEWICZ, A. (1978). Testing of fibre bond strength in cement matrix. Proc. RILEM Symp. Testing and test methods of fibre cement composities, 5–7 Sept. 1978, Sheffield. The Construction Press, Lancaster, pp. 355–365.

DONKER, L. (1979). The effect of fibre segregation on the modulus of rupture of FRC beams reinforced with three different types of fibres (in Dutch). Stev. Rep. 1-79-4, July, Delft.

HANNANT, D. J. (1978). Fibre cements and fibre concretes, Wiley, New York.

HUGHES, B. P. and G. P. CHAPMAN, (1965). Direct tensile test for concrete using modern adhesives. RILEM Bull., 26 March, pp. 77–80.

HUGHES, B. P. and N. I. FATTUHI,(1975). Fibre bond strength in cement and concrete. Mag. Concr. Res., 27, 92, Sept., pp. 161–166.

JOHNSTON, C. D. and R. A. COLEMAN (1974). Strength and deformation of steel fibre reinforced mortar in uniaxial tension. ACI Spec. publ. SP-40, pp. 177–188.

36

KASPERKIEWICZ, J., B. MALMBERG and A. SKARENDAHL, (1978). Determination of fibre content, distribution and orientation in steel fibre concrete by X-ray technique. Proc. RILEM Symp. Testing and test methods of fibre cement composites, 5–7 Sept., 1978, Sheffield. The Construction Press, Lancaster, pp. 297–314.

MAAGE, M. (1976). Bond properties between steel fibre and cement paste, mortar and concrete. Ph.D. Thesis Univ. Trondheim, Div. Build. Mat., Norway Inst. Techn., Trondheim.

MOENS, J. and D. NEMEGEER, (1978). Proc. RILEM Symp. Testing and test methods of fibre cement composites, 5–7 Sept., 1978, Sheffield. The Construction Press, Lancaster, pp. 389–397.

NAAMAN, A. E., F. MOAVENZADEH and J. McGARRY (1974). Probabilistic analysis of fibre reinforced concrete, J. Eng. Mech. Div. A.S.C.E., EM 2, April, pp. 397–413.

NAAMAN, A. E. and S. P. SHAH (1975). Bond studies on oriented and aligned steel fibres. RILEM Symp. Fibre reinforced cement and concrete, 14–17 Sept., 1975, London. The Construction Press, Lancaster, pp. 171–185.

PINCHIN, D. J. (1977). The steel-cement interface: friction and adhesion. Ph.D. Thesis, Univ. Cambridge.

SHAH, S. P. and B. V. RANGAN (1971). Fibre reinforced concrete properties. J. Am. Concr. Inst., Febr., pp. 126–135.

SHAH, S. P., P. STROEVEN, D. DALHUISEN and P. VAN STEKELENBURG, (1978). Complete stress strain curves for steel fibre reinforced concrete in uniaxial tension and compression. Proc. RILEM Symp. Testing and test methods of fibre cement composites, 5–7 Sept., Sheffield. The Construction Press, Lancaster, pp. 399–408.

STROEVEN, P. (1977). The analysis of fibre distributions in fibre reinforced cementitious materials. J. Microsc., Vol. III, Pt. 3, Dec., pp. 283–295.

STROEVEN, P. and S. P. SHAH, (1978). Use of radiography-image analysis for steel fibre reinforced concrete. Proc. RILEM Symp. Testing and test methods of fibre cement composites, 5–7 Sept., 1978, Sheffield. The Construction Press, Lancaster, pp. 275–288.

STROEVEN, P. (1978). Closure on paper by P. Stroeven and S. P. Shah (1978). Proc. RILEM Symp. Testing and test methods of fibre cement composites, 5–7 Sept., 1978, Sheffield. The Construction Press, Lancaster, pp. 308–311.

STROEVEN, P., S. P. SHAH, Y. M. DE HAAN and C. BOUTER, (1978). Pull-out tests of steel fibres. Proc. RILEM Symp. Testing and test methods of fibre cement composites, 5–7 Sept., 1978, Sheffield. The Construction Press, Lancaster, pp. 345–353.

STROEVEN, P. (1979). Morphometry of fibre reinforced cementitious materials. Part II: Inhomogeneity, segregation and anisometry of partially oriented fibre structures. Mat. & Constr., 12, 67, pp. 9–20.

STROEVEN, P. (1980a). Tensile behaviour of fibre reinforced cementitious materials as affected by fibre distribution parameters. Proc. Fifth int. congr. for stereology, 3–8 Sept. 1979, Salzburg. To be published.

STROEVEN, P. (1980b). Morphological study of three types of FRC specimens. Stev. Rep. To be published.

STROEVEN, P. and D. DALHUISEN, (1980). Experimental investigations of the mechanical behaviour of three types of FRC specimens in direct tension. Stev. Rep. To be published.

SWAMY, R. N., P. S. MANGAT and C. V. S. K. RAO, (1974). The mechanics of fibre reinforcement of cement matrices. ACI Spec. publ. SP-44, pp. 1–28.

SWAMY, R. N. and H. STAVRIDES, (1975). Theories of fibre cement and fibre concrete. RILEM Symp. Fibre reinforced cement and concrete, 14–17 Sept., 1975, London. The Construction Press, Lancaster, pp. 197–208.

CUR-VB (1977). CUR Rep. 89. New types of concrete: steel fibre concrete (in Dutch). Stichting Commissie voor uitvoering van research.

7 Notations*

a	aspect ratio of fibres
d	diameter of a fibre, mm
f_i	fineness modulus of sand
l	length of a fibre, mm
l_i	(average)embedment length of fibres in a normal direction to the crack plane, mm
l^*	prediction for the average embedment length obtained from the stress-strain diagram, mm
s	measuring length, mm
wc	water to cement ratio
A	surface area of a cross-section, mm^2
E_c	Young's modulus of the composite, N/mm^2
G	toughness, Nmm
G_s	G/s, specific toughness, N/mm
L	total fibre length, mm
L_v	$= L/V$, mm^{-2}
N	number of fibres
N_A	$= N/A$, mm^{-2}
P	load, N
P_a	load at crack initiation (LOP), N
P_u	ultimate load, N
S	embedded surface area of fibres, mm^2
V	sample volume, mm^3
V_f	volume fraction of fibres
δ_{Pu}	crack width at ultimate load, mm
ε	strain
σ	stress, N/mm^2
σ_u	ultimate tensile strength (UTS), N/mm^2
σ_{us}	ultimate strength of the composite in splitting tension, N/mm^2
σ_{ut}	ultimate strength of the composite in uniaxial tension, N/mm^2
σ_{ut_0}	ultimate tensile strength of the matrix, N/mm^2
τ_a	interfacial shear strength at LOP, N/mm^2
τ_f	dynamic interfacial friction resistance, N/mm^2
τ_{max}	maximum interfacial shear strength at UTS, N/mm^2

* Notations are given here as far as they do not clearly follow from the text.

8 Appendix

A1 Fibre geometry
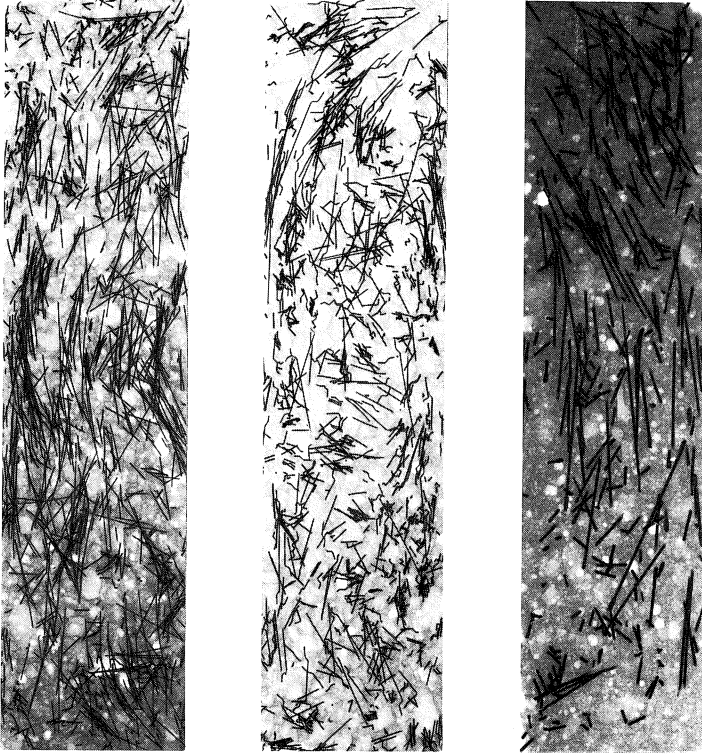
Fig. A1. X-ray radiographs of thin elements of FRC specimens containing the three applied commercial fibre types. From left to right: the straight, hooked and paddled fibres, respectively.

A2 Segregation data

A. Fibre inhomogeneity and anisometry in transverse direction.
    Specimen 1131 (wc = 0.35, f_i = 3.27, paddled fibres): average of 10 sections

$$\left.\begin{array}{l} \omega_t = 0.545 \\ \omega_b = 0.624 \end{array}\right\} \bar{\omega} = 0.58 \qquad \frac{\omega_b}{\omega_t} = 1.15$$

$$\left.\begin{array}{l} L_{v_t} = 0.0258 \ (\text{mm}^{-2}) \\ L_{v_b} = 0.0502 \ (\text{mm}^{-2}) \end{array}\right\} \bar{L}_v = 0.0380 \ (\text{mm}^{-2}) \qquad \frac{L_{v_b}}{L_{v_t}} = 1.95$$

B. Fibre inhomogeneity in axial direction

39

Specimen 2123 (straight fibres)   Specimen 1132 (paddled fibres)
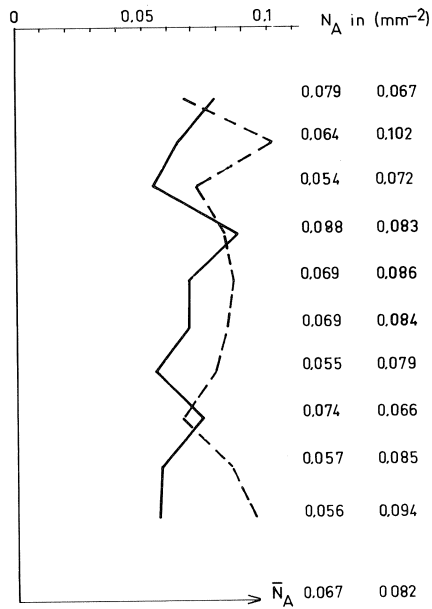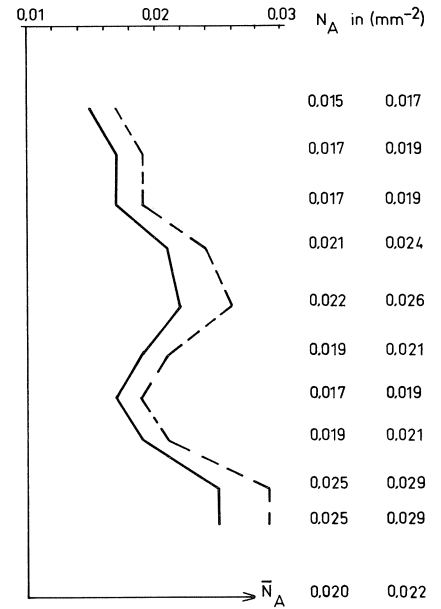

Fig. A2.   Variation of the number of fibres per unit of area along the specimen axis. Comparison
of two quantitative image analysis techniques. The solutions are based on the partially
planar-oriented structural model for the fibre dispersion in the specimen. The feature
counting was executed over the entire cross section, whereas the intersection counting
omitted the most severely disturbed areas near the casting (viz. e.g. Stroeven [1979]).
The presented examples are two extreme cases.